

Direct dynamics simulation of dioxetane formation and decomposition via the singlet $\cdot\text{O}-\text{O}-\text{CH}_2-\text{CH}_2\cdot$ biradical: Non-RRKM dynamics

, , [Wibe A. de Jong](#), [Hans Lischka](#), [Theresa L. Windus](#), and [William L. Hase](#)

Citation: *J. Chem. Phys.* **137**, 044305 (2012); doi: 10.1063/1.4736843

View online: <http://dx.doi.org/10.1063/1.4736843>

View Table of Contents: <http://aip.scitation.org/toc/jcp/137/4>

Published by the [American Institute of Physics](#)

Direct dynamics simulation of dioxetane formation and decomposition via the singlet $\cdot\text{O}-\text{O}-\text{CH}_2-\text{CH}_2\cdot$ biradical: Non-RRKM dynamics

Rui Sun (孙睿),¹ Kyoyeon Park (박교연),^{1,2} Wibe A. de Jong,³ Hans Lischka,¹ Theresa L. Windus,⁴ and William L. Hase¹

¹Department of Chemistry and Biochemistry, Texas Tech University, Lubbock, Texas 79409, USA

²Department of Chemistry and Biochemistry, University of California, San Diego, La Jolla, California 92093, USA

³Environmental Molecular Science Laboratory, Pacific Northwest National Laboratory, Richland, Washington 99352, USA

⁴Department of Chemistry, Iowa State University, Ames, Iowa 50011, USA

(Received 18 March 2012; accepted 28 June 2012; published online 26 July 2012)

Electronic structure calculations and direct chemical dynamics simulations are used to study the formation and decomposition of dioxetane on its ground state singlet potential energy surface. The stationary points for $^1\text{O}_2 + \text{C}_2\text{H}_4$, the singlet $\cdot\text{O}-\text{O}-\text{CH}_2-\text{CH}_2\cdot$ biradical, the transition state (TS) connecting this biradical with dioxetane, and the two transition states and gauche $\cdot\text{O}-\text{CH}_2-\text{CH}_2-\text{O}\cdot$ biradical connecting dioxetane with the formaldehyde product molecules are investigated at different levels of electronic structure theory including UB3LYP, UMP2, MRMP2, and CASSCF and a range of basis sets. The UB3LYP/6-31G* method was found to give representative energies for the reactive system and was used as a model for the simulations. UB3LYP/6-31G* direct dynamics trajectories were initiated at the TS connecting the $\cdot\text{O}-\text{O}-\text{CH}_2-\text{CH}_2\cdot$ biradical and dioxetane by sampling the TS's vibrational energy levels, and rotational and reaction coordinate energies, with Boltzmann distributions at 300, 1000, and 1500 K. This corresponds to the transition state theory model for trajectories that pass the TS. The trajectories were directed randomly towards both the biradical and dioxetane. A small fraction of the trajectories directed towards the biradical recrossed the TS and formed dioxetane. The remainder formed $^1\text{O}_2 + \text{C}_2\text{H}_4$ and of these $\sim 40\%$ went directly from the TS to $^1\text{O}_2 + \text{C}_2\text{H}_4$ without getting trapped and forming an intermediate in the $\cdot\text{O}-\text{O}-\text{CH}_2-\text{CH}_2\cdot$ biradical potential energy minimum, a non-statistical result. The dioxetane molecules which are formed dissociate to two formaldehyde molecules with a rate constant two orders of magnitude smaller than that predicted by Rice–Ramsperger–Kassel–Marcus theory. The reaction dynamics from dioxetane to the formaldehyde molecules do not follow the intrinsic reaction coordinate or involve trapping in the gauche $\cdot\text{O}-\text{CH}_2-\text{CH}_2-\text{O}\cdot$ biradical potential energy minimum. Important non-statistical dynamics are exhibited for this reactive system. © 2012 American Institute of Physics. [<http://dx.doi.org/10.1063/1.4736843>]

I. INTRODUCTION

The dynamics and kinetics of oxidation reactions are of great interest, especially the reaction of molecular oxygen with hydrocarbons,^{1–3} which plays an important role in both atmospheric⁴ and combustion⁵ chemistry. The reaction kinetics of $^3\text{O}_2$ with unsaturated hydrocarbons have been studied both experimentally^{6–12} and theoretically^{13,14} for alkenes^{6–12,14} and, in particular, for ethylene.^{6,15} The possible importance of $^3\text{O}_2 +$ alkene reactions under combustion conditions has been considered.^{12,15} Also, unsaturated hydrocarbons are constituents in fuels and are expected to undergo exothermic reaction with ground state molecular oxygen, $^3\text{O}_2$, possibly contaminating the fuel. In order to understand possible mechanisms for molecular oxygen reactions with unsaturated hydrocarbons, both $^3\text{O}_2 + \text{C}_2\text{H}_4$ and $^1\text{O}_2 + \text{C}_2\text{H}_4$ have been studied using various electronic structure theories.^{1,3,15,16} The latter has been studied more extensively than the former. Experimental studies of $^3\text{O}_2$ and $^1\text{O}_2$ reaction with C_2H_4 are quite limited.⁶

There are a large number of pathways on the singlet and triplet potential energy surfaces (PESs) for the reaction between molecular oxygen and ethylene, and the reaction dynamics is complicated by numerous singlet-triplet interactions.^{15,16} From previous studies, one important and possibly dominant pathway for reaction of triplet molecular oxygen and ethylene is



This reaction has a low potential energy barrier and the triplet biradical product may access much lower reaction pathways via a triplet-singlet transition. The singlet biradical, formed by intersystem crossing, undergoes ring-closure via a transition state (TS) to form dioxetane (DO).

Due to the chemiluminescence during the thermal decomposition of 1,2-dioxetane derivatives, there have been numerous investigations of the mechanism for this process since the early 1970s.^{17–25} Reaction energetics and rate data for

different 1,2-dioxetane derivatives are available as a result of numerous experimental studies.^{17,19} However, the precise nature of the mechanism is still somewhat uncertain. Considerable effort has been made to characterize the potential energy surfaces for DO decomposition and the mechanism for the electronic excitation using electronic structure theories.^{22–25} These theoretical studies indicate that the reaction occurs via a two-step process: first the cleavage of the O–O bond and formation of the $\cdot\text{O}-\text{H}_2\text{C}-\text{CH}_2-\text{O}\cdot$ biradical; and then cleavage of the C–C bond and formation of two formaldehyde molecules. It is suggested that a transition from S_0 to S_1 or T_1 occurs near the barrier for the O–O bond cleavage or near the biradical minimum. However the barrier height for O–O bond cleavage, locations of crossings between different electronic surfaces, and the existence of minima on the excited states are highly dependent on the level of theory used in the *ab initio* calculation. For example, the ring opening reaction of DO to produce the biradical occurs with a very small activation energy of 2.0 kcal/mol with MP2/6-31G**//MCSCF/4-31G,²² a much higher energy of 17.6 kcal/mol with CASPT2(12,10)//CASSCF(12,10)/6-31+G*,²³ and an even higher energy of 24.1 kcal/mol using MS-CASPT2(12,10)/ANO-RCC theory.²⁴ In addition the position of the S_0/T_1 crossing depends on the level of theory. To summarize, these studies have shown that the height of the barrier for DO dissociation to two formaldehyde molecules and the presence and location of the S_0/T_1 crossing are both highly dependent on the electronic structure theory used for the calculations.

For the work presented in this paper a direct dynamics simulation^{26,27} at the UB3LYP/6-31G* level of theory^{28–32} is used to study the atomistic dynamics ensuing from trajectories initiated at the TS connecting the singlet $\cdot\text{O}-\text{O}-\text{CH}_2-\text{CH}_2\cdot$ biradical and DO. This electronic structure method is chosen by comparing with experiments¹⁹ and previous calculations¹⁶ using the CASSCF^{33,34} and MRMP2^{35,36} methods with the aug-pp-cVDZ basis set.³⁷ Canonical sampling at 300, 1000, and 1500 K was used to choose initial conditions for the trajectories, which were propagated randomly in the directions of the singlet $\cdot\text{O}-\text{O}-\text{CH}_2-\text{CH}_2\cdot$ biradical and DO. From the simulations the average lifetime of DO and the DO dissociation path to form formaldehyde are determined. The DO dissociation rate constant obtained from the direct dynamics simulations is compared with that determined from Rice–Ramsperger–Kassel–Marcus (RRKM) theory.³⁸ The simulation results presented here provide information concerning the atomic-level dynamics of DO dissociation on the ground state singlet S_0 PES in the absence of possible transitions to the excited S_1 and T_1 electronic states.

II. COMPUTATIONAL METHODOLOGY

A. Electronic structure calculations and potential energy surface

For a classical trajectory direct dynamics simulation the potential energy gradient, and possibly Hessian as well, are needed for each numerical integration step, which makes

the simulation very expensive in terms of computational time.^{26,27} As a result, an electronic structure theoretical method needs to be selected to make the simulation efficient and feasible, as well as accurate. When experimental information is available it may often be used to assess the accuracy of electronic structure methods. However, for the work presented here, the results from high-level CASSCF and MRMP2 calculations were treated as benchmarks for comparing different methods.¹⁶

Information for the $\text{O}_2 + \text{C}_2\text{H}_4$ singlet PES is obtained from recent work by Park *et al.*,¹⁶ in which the CASSCF/aug-cc-pVDZ level of theory was used to characterize structures and vibrational frequencies, and then MRMP2(12,12)//CASSCF(12,12)/aug-cc-pVDZ single point energies were calculated at the CASSCF geometries for the $^1\text{O}_2 + \text{C}_2\text{H}_4$ separated reactants (SR), the TS (TSa) connecting SR with the $\cdot\text{O}-\text{O}-\text{CH}_2-\text{CH}_2\cdot$ biradical intermediate (IM1-s), IM1-s, the TS (TSb) connecting IM1-s with DO, and DO. For the work presented here, geometry optimizations were performed for these structures using unrestricted second-order Møller–Plesset (UMP2)³⁹ and unrestricted B3LYP (UB3LYP) density functional theory, with basis sets ranging from 6-31G* to 6-311++G**. The CASSCF/aug-cc-pVDZ structures for TSa, IM1-s, TSb, and DO have been given previously,¹⁶ and in Figure 1 the UB3LYP/6-31G* and CASSCF/aug-cc-pVDZ structures for TSa, IM1-s, TSb, and DO are compared. The UMP2 and UB3LYP stationary point structures, with the 6-31G* and 6-311++G** basis sets, are listed in Table I, where they are compared with the CASSCF/aug-cc-pVDZ structures.

Energies for SR, TSa, IM1-s, TSb, and DO are listed in Table II for the different theoretical methods and basis sets. The UB3LYP energies are in overall good agreement with those given by the MRMP2(12,12)//CASSCF(12,12)/aug-cc-pVDZ method. The UB3LYP/6-31G* relative energies, with respect to DO, are 47.9 and 37.5 kcal/mol for TSb and IM1-s, respectively, which are only slightly higher than the respective MRMP2(12,12) values of 44.6 and 36.5 kcal/mol reported by Park *et al.*¹⁶ In the study of Maranzana *et al.*,³ these energies were reported as 48.1 and 40.0 kcal/mol using the (10,10)//CAS-MCSCF(10,10)/6-31G* method. The UB3LYP energies are overall independent of the size of the basis set. The energy barrier from IM1-s to TSb increases from 10.4 to 11.0 kcal/mol as the basis set size increases from 6-31G* to 6-311++G**. The MRMP2 benchmark barrier is 8.1 kcal/mol. The UMP2 method does not provide accurate results for this system, greatly underestimating the IM1-s \rightarrow TSb barrier.

The MRMP2 barrier is substantially lower than those given by UB3LYP and CASSCF for $^1\text{O}_2 + \text{C}_2\text{H}_4$ addition to form IM1-s. This arises in part from the difficulty of these latter theories to correctly describe the electronic structure of $^1\text{O}_2$. However, as discussed previously,¹⁶ the low MRMP2 barrier for this reaction appears to also arise from different MRMP2 and CASSCF structures for TSa. Calculating MRMP2 energies, along the CASSCF intrinsic reaction coordinate (IRC) connecting $^1\text{O}_2 + \text{C}_2\text{H}_4$ with IM1-s, yields a barrier at a O_2-C_3 distance of 1.997 Å and longer than the value of 1.862 Å at the CASSCF barrier. The value of the

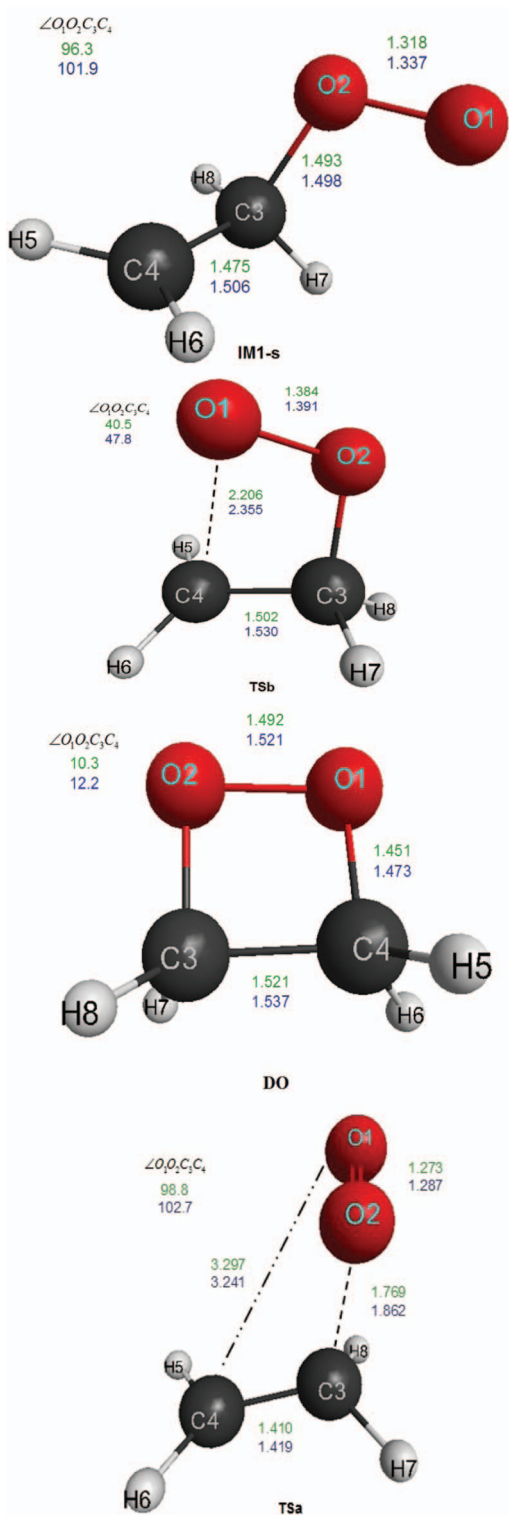


FIG. 1. UB3LYP//6-31G* optimized structures of the transition state (Tsa), $\cdot\text{O}-\text{O}-\text{CH}_2-\text{CH}_2\cdot$ biradical intermediate (IM1-s), transition state (Tsb), and dioxetane (DO) for the singlet PES. Bond distances and angles are in units of angstroms and degrees, respectively. The lower values are obtained from CASSCF/aug-cc-pVDZ theory.¹⁶

resulting MRMP2 barrier is 10.2 kcal/mol for $^1\text{O}_2 + \text{C}_2\text{H}_4 \rightarrow \text{IM1-s}$ and 10.5 kcal/mol for $\text{IM1-s} \rightarrow ^1\text{O}_2 + \text{C}_2\text{H}_4$. The latter is markedly higher than the UB3LYP values of 3.2 and 3.5 kcal/mol for the aug-cc-pVDZ and 6-31G* basis set,

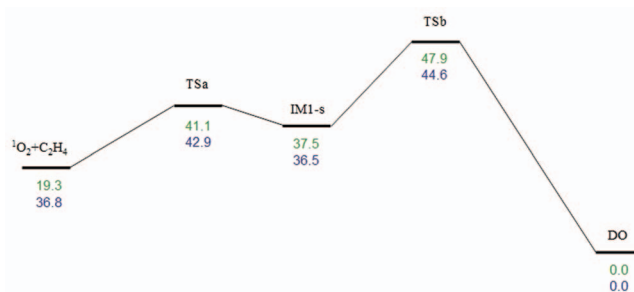


FIG. 2. Depiction of the UB3LYP/6-31G* energies (kcal/mol), green, for $^1\text{O}_2 + \text{C}_2\text{H}_4$ (SR), transition state TSa, the $\cdot\text{O}-\text{O}-\text{CH}_2-\text{CH}_2\cdot$ biradical intermediate IM1-s, transition state TSb, and dioxetane (DO). The lower energies, blue, are the MRMP2//CASSCF/aug-cc-pVDZ values.¹⁶

respectively. The UB3LYP/aug-cc-pVDZ value for the O_2-C_3 distance at the TSa is 1.768 Å and much closer to the above CASSCF value than that for MRMP2. In assessing those CASSCF, MRMP2, and UB3LYP properties for TSa, it is of interest to note that MP2 and B3LYP treat dynamic correlation, while CASSCF treats static correlation.

As described above the UB3LYP barriers for $^1\text{O}_2 + \text{C}_2\text{H}_4 \rightarrow \text{IM1-s}$ are ~ 20 kcal/mol and much higher than the MRMP2 value of ~ 10 kcal/mol. However, of interest in this study are the dynamics from TSb to form dioxetane and the singlet biradical. UB3LYP gives good energies for these processes, making it acceptable for the direct dynamics simulations. The UB3LYP/6-31G* potential energies along the $\text{SR} \rightarrow \text{TSa} \rightarrow \text{IM1-s} \rightarrow \text{TSb} \rightarrow \text{DO}$ reaction path are depicted in Figure 2, where they are compared with the MRMP2//CASSCF/aug-cc-pVDZ energies.

As shown in Table I and Figure 1, the UB3LYP geometries are in good agreement with those from the CASSCF/aug-cc-pVDZ calculations, although UB3LYP gives “tighter” bond lengths. An essential internal coordinate in the $\text{IM1-s} \rightarrow \text{TSb} \rightarrow \text{DO}$ reaction path is the $\text{O}_1\text{O}_2\text{C}_3\text{C}_4$ dihedral angle whose UB3LYP/6-31G* value is 96.3°, 40.5°, and 10.3° for IM1-s, Tsb and DO, respectively. These respective values are only 5.6°, 7.3°, and 1.9° less than those given by the CASSCF calculation.

Dioxetane has a dissociation path to two formaldehyde molecules on the singlet PES. The IRC⁴³ for this pathway, as given by UB3LYP/6-31G* theory, is shown in Figure 3. There are two transition states and one gauche $\cdot\text{O}-\text{CH}_2-\text{CH}_2-\text{O}\cdot$ minimum along this pathway. The structures of the two transition states TS1 and TS2 are shown in Figure 4. The energies of TS1, the minimum, and TS2 are, respectively, 20.9, 8.9, and 9.2 kcal/mol with respect to DO.

The UB3LYP/6-31G* 0 K activation energy for DO dissociation (TS1) is 20.9 kcal/mol and changes to 18.5 kcal/mol with a zero-point energy (ZPE) correction included. This energy is in approximate agreement but somewhat lower than the value of 22.7 ± 0.8 kcal/mol measured by Adam and Baader at 333 K.¹⁹ Wilsey *et al.*²³ have studied the same system using CASPT2(12,10)//CASSCF(12,10)/6-31+G*. They also found two transition states with structures similar to those reported here. For example, the $\text{O}_1\text{C}_4\text{C}_3\text{O}_2$ dihedral angle, $\text{O}_2\text{C}_3\text{C}_4$ bond angle, and O_1-O_2 bond length in TS1 from their calculation are 33°, 99°, and 2.118 Å,

TABLE I. Comparison of IM1-s, TSb, and DO structures with different electronic structure methods.^a

| | IM1-s (biradical intermediate) | | | | | | | |
|--------------------|--------------------------------|-------------------------------|-------------------------------|-------------------------------|--|--|---|---|
| | Bond length | | | | Angle | | Dihedral | |
| | O ₁ O ₂ | O ₂ C ₃ | C ₃ C ₄ | O ₁ C ₄ | O ₁ O ₂ C ₃ | O ₁ C ₃ C ₄ | O ₁ O ₂ C ₃ C ₄ | O ₁ O ₂ C ₃ H ₇ |
| UB3LYP/6-31G* | 1.318 | 1.493 | 1.475 | 3.136 | 111.7 | 108.6 | 96.3 | 26.4 |
| UB3LYP/6-311++G** | 1.313 | 1.495 | 1.473 | 3.155 | 112.5 | 108.4 | 97.9 | 24.8 |
| UMP2/6-31G* | 1.310 | 1.472 | 1.480 | 2.984 | 110.2 | 109.8 | 82.8 | 40.6 |
| UMP2/6-311++G** | 1.338 | 1.497 | 1.507 | 3.178 | 110.9 | 106.6 | 100.8 | 21.4 |
| CASSCF/aug-cc-pVDZ | 1.337 | 1.498 | 1.506 | 3.189 | 111.0 | 106.5 | 101.9 | 20.3 |
| | TSb (Transition state) | | | | | | | |
| | Bond length | | | | Angle | | Dihedral | |
| | O ₁ O ₂ | O ₂ C ₃ | C ₃ C ₄ | O ₁ C ₄ | O ₁ O ₂ C ₃ | O ₂ C ₃ C ₄ | O ₁ O ₂ C ₃ C ₄ | O ₁ O ₂ C ₃ H ₇ |
| UB3LYP/6-31G* | 1.384 | 1.441 | 1.502 | 2.206 | 99.6 | 101.6 | 40.5 | 78.3 |
| UB3LYP/6-311++G** | 1.383 | 1.441 | 1.500 | 2.208 | 100.0 | 101.5 | 40.1 | 78.7 |
| UMP2/6-31G* | 1.313 | 1.473 | 1.481 | 2.897 | 110.3 | 111.5 | 70.5 | 53.4 |
| UMP2/6-311++G** | 1.298 | 1.467 | 1.483 | 2.885 | 111.2 | 111.7 | 68.6 | 55.3 |
| CASSCF/aug-cc-pVDZ | 1.391 | 1.464 | 1.530 | 2.355 | 100.0 | 102.9 | 47.8 | 71.5 |
| | DO (Dioxetane) | | | | | | | |
| | Bond length | | | | Angle | | Dihedral | |
| | O ₁ O ₂ | O ₂ C ₃ | C ₃ C ₄ | O ₁ C ₄ | O ₁ O ₂ C ₃ | O ₂ C ₃ C ₄ | O ₁ O ₂ C ₃ C ₄ | O ₁ O ₂ C ₃ H ₇ |
| UB3LYP/6-31G* | 1.492 | 1.452 | 1.520 | 1.451 | 89.0 | 90.1 | 10.3 | 102.8 |
| UB3LYP/6-311++G** | 1.488 | 1.454 | 1.519 | 1.453 | 88.9 | 88.7 | 12.0 | 100.4 |
| UMP2/6-31G* | 1.520 | 1.458 | 1.509 | 1.458 | 88.2 | 88.6 | 18.4 | 93.0 |
| UMP2/6-311++G** | 1.502 | 1.452 | 1.511 | 1.452 | 88.4 | 88.0 | 19.7 | 91.3 |
| CASSCF/aug-cc-pVDZ | 1.521 | 1.473 | 1.537 | 1.473 | 89.6 | 89.0 | 12.2 | 99.8 |

^aDistances are in angstroms and angles in degrees.TABLE II. Relative stationary point energies for the ¹O₂ + C₂H₄ → TSb pathway.^a

| | SR ^b | TSa | IM1-s | TSb |
|-----------------------------|-----------------|------|-------|------|
| UB3LYP/6-31G* | 19.3 | 41.1 | 37.5 | 47.9 |
| UB3LYP/6-31G** | 18.7 | 40.8 | 37.3 | 47.7 |
| UB3LYP/6-31+G* | 18.0 | 40.1 | 36.3 | 46.8 |
| UB3LYP/6-31+G** | 17.2 | 39.7 | 36.0 | 46.6 |
| UB3LYP/6-31++G** | 17.3 | 39.7 | 36.0 | 46.5 |
| UB3LYP/6-311++G** | 14.0 | 38.0 | 35.0 | 46.0 |
| UMP2/6-31G* | 21.4 | 71.4 | 51.5 | 52.3 |
| UMP2/6-31G** | 22.0 | 71.1 | 51.5 | 53.9 |
| UMP2/6-31+G* | 22.3 | 71.1 | 51.3 | 52.2 |
| UMP2/6-31+G** | 11.4 | 60.4 | 40.8 | 41.8 |
| UMP2/6-31++G** | 11.5 | 60.5 | 40.9 | 41.8 |
| UMP2/6-311++G** | 6.7 | 56.4 | 37.4 | 38.2 |
| SPMRMP2(8,8) ^c | | | 37.9 | 44.8 |
| SPMRMP2(12,12) ^c | 36.8 | 42.9 | 36.5 | 44.6 |
| CASSCF(8,8) ^c | | | 53.6 | 54.9 |
| CASSCF(12,12) ^c | 27.9 | 56.7 | 45.8 | 53.0 |

^aEnergies are in kcal/mol and with respect to dioxetane (DO). The stationary points are identified as in Ref. 16. The energies of SR, TSa, IM1-s, and TSb for the UB3LYP/aug-cc-pVDZ theory are 18.4, 39.2, 36.0, and 46.5 kcal/mol, respectively; i.e., Ref. 16.^bSR represents ¹O₂ + C₂H₄ separated reactants.^cResults are from Ref. 16. The MRMP2 energies are single point energies calculated at the CASSCF(8,8) and CASSCF(12,12) geometries calculated with the aug-cc-pVDZ basis set.

respectively, compared to 29.5°, 97.5°, and 2.011Å found here with UB3LYP/6-31G*. The 0 K activation energy for DO dissociation reported by Wilsey *et al.*²³ is 17.6 kcal/mol (16.3 kcal/mol with ZPE correction), which still underestimates the experimental value. In a more recent study, using MS-CASPT2(12,10)/ANO-RCC theory, De Vico *et al.*²⁴

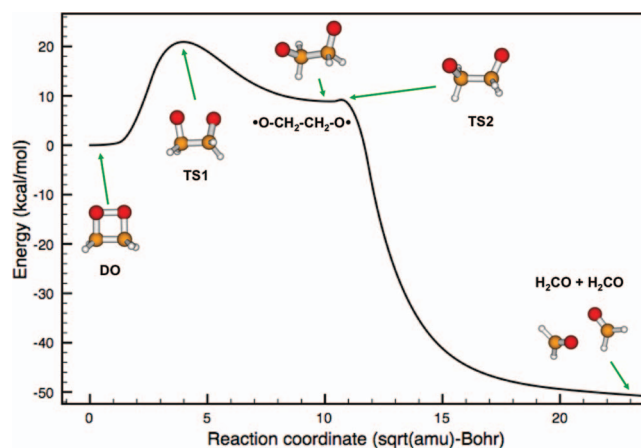


FIG. 3. UB3LYP/6-31G* potential energy along the IRC for dissociation of dioxetane.

TABLE III. Relative stationary point energies for the dioxetane \rightarrow 2 H₂CO pathway.

| Theory | Property ^a | | | Energy |
|---|-----------------------|-------|-------------|------------|
| | C–C | O–O | Twist angle | |
| DO | | | | |
| UB3LYP/6-31G* | 1.521 | 1.492 | 10.3 | 0 |
| MS-CASPT2(12,10) ^b | 1.529 | 1.578 | 15.4 | 0 |
| MS-CASPT2(12,10) ^c | 1.511 | 1.510 | 16.8 | 0 |
| CASPT2(12,10) ^d | 1.538 | 1.554 | 9 | 0 |
| Experiment | ... | ... | ... | 0 |
| TS1 | | | | |
| UB3LYP/6-31G* | 1.519 | 2.011 | 29.5 | 20.9 |
| MS-CASPT2(12,10) ^b | 1.536 | 2.262 | 37.1 | 23.5 |
| MS-CASPT2(12,10) ^c | 1.510 | 2.288 | 43.1 | 24.1 |
| CASPT2(12,10) ^d | 1.533 | 2.118 | 33 | 17.6 |
| Experiment ^e | ... | ... | ... | 22.7 ± 0.8 |
| ·O–CH ₂ –CH ₂ –O· | | | | |
| UB3LYP/6-31G* | 1.546 | 2.965 | 62.4 | 8.9 |
| MS-CASPT2(12,10) ^b | 1.546 | 3.016 | 68.3 | 17.9 |
| MS-CASPT2(12,10) ^f | ... | ... | ... | ... |
| CASPT2(12,10) ^d | 1.560 | 2.933 | 76 | 13.4 |
| TS2 | | | | |
| UB3LYP/6-31G* | 1.596 | 2.956 | 64.7 | 9.2 |
| MS-CASPT2(12,10) ^b | ... | ... | ... | ... |
| MS-CASPT2(12,10) ^f | ... | ... | ... | ... |
| CASPT2(12,10) ^d | 1.632 | 2.922 | 73 | 13.4 |

^aDistances are in angstrom, angles are in degree and energies are in kcal/mol. The energies of the stationary points are relative energies respect to DO.

^bSingle point calculation of the CASSCF/ANO-RCC geometry. From Ref. 24.

^cCalculation with the ANO-RCC basis set. From Ref. 24.

^dSingle point calculation at the CASSCF(12,10)/6-31+G* geometry. From Ref. 23.

^eFrom Ref. 19.

^fNot reported.

located TS1 and found it to be 24.1 kcal/mol higher than the DO minimum.

Electronic structure calculations of stationary point structures and energies for the DO \rightarrow 2H₂CO dissociation pathway are summarized in Table III. The energy of TS1, the dissociation energy, and its structure are similar for the current UB3LYP calculations and previous CASPT2 and MS-CASPT2 calculations. The UB3LYP and CASPT2 energies and structures are also in overall good agreement for the ·O–CH₂–CH₂–O· biradical and TS2. It is noteworthy that UB3LYP predicts the biradical to be 0.3 kcal/mol lower in energy than for TS2, while CASPT2 predicts that these species are essentially isoenergetic. As a result of these comparisons, UB3LYP/6-31G* theory gives an acceptable representation of the pathway for dissociation of DO to formaldehyde. After considering its accuracy and computational expense, UB3LYP/6-31G* was chosen as a model for the direct dynamics simulations reported here.

B. Classical trajectory direct dynamics simulation

1. Integrating the classical equations of motion

Classical trajectory simulations have been widely used to study unimolecular and intramolecular dynamics since the early 1960s.^{44,45} Important atomic-level chemical dynamics

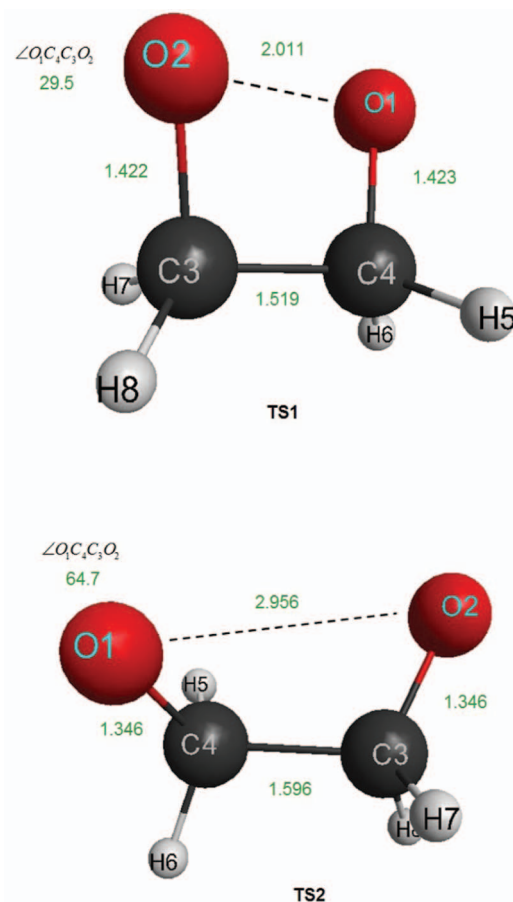


FIG. 4. UB3LYP/6-31G* optimized structure of the two transition states (TS1 and TS2) for dioxetane dissociation to two formaldehyde molecules. Bond distances and dihedral angles are in units of angstroms and degrees.

information such as reaction pathways, unimolecular rate constants,⁴⁶ intramolecular vibrational energy redistribution rates,⁴⁷ etc. may be obtained from the simulations. A broadly applicable approach for performing the simulations is to use Born-Oppenheimer direct dynamics^{26,27} for which the potential energy and its gradient, needed to solve the classical equations of motion, are obtained directly from an electronic structure theory.

Various algorithms are used to integrate the classical equations of motion. To minimize the computational expense of a direct dynamics simulation it is important to use the largest integration time step as possible, while maintaining the accuracy of the trajectory. Symplectic methods typically give good energy conservation for long time trajectory integrations with large integration time steps, since certain dynamical properties such as the phase-space volume are well preserved.⁴⁸ The most widely used symplectic integrators are the fourth-order Verlet and velocity-Verlet,⁴⁹ and sometimes a sixth-order integrator for a higher stability requirement.⁵⁰ At each integration step for a direct dynamics trajectory, the molecular orbitals (MOs) obtained for the previous integration step are used to initiate the self-consistent field⁵¹ procedure for the current electronic structure calculation. These MOs are expected to be similar to the current ones, enhancing the efficiency of the electronic structure calculation and the direct dynamics simulation.

All the methods and algorithms for the classical trajectory simulations reported here are compiled in the computational code VENUS.^{52,53} NWCHEM⁵⁴ and GAMESS⁵⁵ are the electronic structure theory codes coupled with VENUS for the direct dynamics simulations. The integration time step is 0.3 fs and the integration method is velocity-Verlet. Each trajectory was integrated for a maximum time of 4.5 ps and the average energy fluctuation is 0.3, 0.6, and 0.7 kcal/mol for the simulations at 300, 1000, and 1500 K, respectively. These fluctuations are less than 1% of the total energy.

As discussed above in the Introduction, there are several electronic states with energies similar to that for the ground state singlet PES studied here. These effects are particularly important for the IM1-s and TS1/TS2 regions of this PES. Substantial care was taken to assure that the trajectories remained on this PES. The S2 value was followed to assure that it changed smoothly between values for open- and closed-shell structures on the PES. As discussed above, energy conservation was carefully checked. When the trajectories were halted, they had either correctly dissociated to $^1\text{O}_2 + \text{C}_2\text{H}_4$ or 2 H_2CO , or remained as DO. The wavefunctions were checked, for the trajectories that formed DO and did not dissociate to two formaldehydes, to assure the trajectories remained on the ground state singlet PES.

2. Trajectory initial conditions and trajectory analyses

The simulations were performed to study the ensuing dynamics for trajectories initiated at TSb, which as discussed above connects the singlet $\cdot\text{O}-\text{O}-\text{CH}_2-\text{CH}_2\cdot$ biradical IM1-s with DO. This TS may be accessed by $^1\text{O}_2 + \text{C}_2\text{H}_4$ collisions and by $^3\text{O}_2 + \text{C}_2\text{H}_4$ collisions with a triplet/singlet electronic non-adiabatic transition. The previous electronic structure calculation¹⁶ for the triplet and singlet PESs found that the triplet and singlet $\cdot\text{O}-\text{O}-\text{CH}_2-\text{CH}_2\cdot$ biradicals IM1 and IM1-s formed by O_2 addition to C_2H_4 are nearly isoenergetic. The minimum energy crossing point and crossing seam, for $^3\text{O}_2 + \text{C}_2\text{H}_4$ collisions, is in this region of the triplet and singlet PESs and is where the triplet/singlet electronic non-adiabatic transition for these collisions is expected to occur. For TSb, which connects singlet $\cdot\text{O}-\text{O}-\text{CH}_2-\text{CH}_2\cdot$ with DO, the triplet PES is much higher in energy than the singlet PES.

The trajectories were initiated at TSb with canonical Boltzmann sampling. This model assumes that transition state theory (TST) is valid for the IM1-s \rightarrow DO kinetics.²⁶ The accuracy of TST for reactive system with electronic non-adiabatic transitions has been considered previously.^{56,57} For the current model study of $^3\text{O}_2 + \text{C}_2\text{H}_4 \rightarrow \text{IM1} \rightarrow \text{IM1-s} \rightarrow \text{TSb} \rightarrow \text{DO}$ three assumption are critical: i.e., recrossing of TSb are unimportant,⁵⁸ which is supported by the direct dynamics simulations reported below; triplet/singlet electronic transitions are insignificant for TSb-like structures, as found from the previous electronic structure calculations for the triplet and singlet PESs;¹⁶ and a Boltzmann distribution of reactant states is maintained on the singlet PES preceding TSb.⁵⁸ This latter assumption has received considerable discussion and will only be violated if reaction is so fast that

reactant collisions cannot maintain a Boltzmann distribution of states for the reactants.⁵⁸

By initiating the trajectories at TSb, proper ZPE conditions for the TS are enforced and the efficiency of the direct dynamics simulation is enhanced. If the trajectories were initiated at IM1-s they would not have the proper ZPE conditions as they crossed TSb and substantial integration time would be used to propagate the motion from IM1-s to TSb. Previous work has shown that TS sampling gives simulation results in good agreement with experiment, if the kinetics is described by TST.^{26,59}

Initial conditions are chosen at TSb for temperatures T of 300, 1000, and 1500 K. The vibrational energies for the TS normal modes are sampled from a Boltzmann distribution at temperature T .³⁸ The quantum number n_i in the i^{th} mode is sampled using the probability distribution

$$P(n_i) = \exp(-n_i h\nu_i / k_b T_{\text{vib}}) [1 - \exp(-h\nu_i / k_b T_{\text{vib}})], \quad (2)$$

for which ν_i is the vibrational frequency of the i^{th} mode. The rotational energy is chosen from a thermal distribution for a symmetric top at certain temperature using the algorithm developed by Bunker and Goring-Simpson⁶⁰ The reaction coordinate translational energy was sampled so that its average value is RT .⁶¹

The harmonic vibrator/rigid rotor model of RRKM theory³⁸ was used to calculate the rate constant for DO decomposing to two formaldehyde molecules. The DO energy E for the RRKM calculation is the average vibrational, reaction coordinate translational, and rotational energy of TSb plus the potential energy release in going from TSb to DO. The former is

$$\langle E_{\text{TSb}}(T) \rangle = \langle E^{\text{vib}}(T) \rangle + RT + 3RT/2. \quad (3)$$

Both classical and quantum RRKM calculations were performed for DO decomposition. For the classical calculation E is the sum of $\langle E_{\text{TSb}}(T) \rangle$, Eq. (3), the ZPE of TSb, and the classical potential energy difference between TSb and DO; i.e., $E = \langle E_{\text{TSb}}(T) \rangle + 83.8$ kcal/mol. For the quantum calculation E is the sum of $\langle E_{\text{TSb}}(T) \rangle$ and the difference in the potential energies of the ZPE levels of TSb and DO; i.e., $E = \langle E_{\text{TSb}}(T) \rangle + 44.8$ kcal/mol. The classical values of E are 86.2, 101.6, and 117.0 kcal/mol, for the simulation temperatures of 300, 1000, and 1500 K, respectively. The respective quantum values of E are 47.2, 62.6, and 78.1 kcal/mol.

The RRKM rate constant $k(E, J)$ is given by³⁸

$$k(E, J) = N^\ddagger(E, J) / h\rho(E, J). \quad (4)$$

$N^\ddagger(E, J)$ is the sum of states for TS1, given by $\sum N^\ddagger[E - E_0 - E_r^\ddagger(J, K)]$, and $\rho(E, J)$ is the density of states for DO, given by $\sum \rho[E - E_r(J, K)]$. The summations are for K from $-J$ to J and E_r is the rotational energy. The energy barrier for dioxetane DO decomposition is E_0 . It is the classical barrier, 20.9 kcal/mol, for the classical RRKM calculation and the difference in the potential energies of the ZPE levels of TS1 and DO, 18.5 kcal/mol, for the quantum RRKM calculation. Angular momentum is conserved in going from TSb and DO, and J is the value for the average rotational energy $3RT/2$ of TSb. The quantum number J equals 33, 60, and 73, respectively,

for the simulations at 300, 1000, and 1500 K. The projection of J onto the z -axis, i.e., the K quantum number, is assumed to be a non-conserved and an active degree of freedom.^{38,62,63} This k_{RRKM} is the microcanonical rate constant for the average energy of the ensemble of trajectories and may be compared with the direct dynamics trajectory rate constant for dioxetane decomposition. Values of k_{RRKM} were calculated with a general RRKM computer program.⁶⁴ The classical values are 3.0×10^{11} , 6.4×10^{11} , and $1.1 \times 10^{12} \text{ s}^{-1}$, for the simulation temperatures of 300, 1000, and 1500 K, respectively. The respective quantum values are 1.7×10^{11} , 4.7×10^{11} , and $9.5 \times 10^{11} \text{ s}^{-1}$. The small difference between the classical and quantum rate constants is expected given the high excitation energy of DO. For the high energy limit the classical and quantum RRKM rate constants become the same.⁶⁵

The trajectories initiated at TSb were integrated up to a maximum time $t_{max} = 4.5 \text{ ps}$. Only a small fraction of the excited dioxetane molecules decompose during the simulations and the trajectory unimolecular rate constant was found from the number of trajectories remaining at t_{max} . The time for the analysis is not t_{max} , but t_{DO} , where the latter is the length of time the intramolecular vibrational dynamics of DO was followed; i.e., see below in Sec. III B

$$N(t_{DO})/N(0) = \exp(-kt_{DO}). \quad (5)$$

The total number of products formed at t_{max} is $P(t_{max}) = N(0) - N(t_{max})$.

III. SIMULATION RESULTS

A total number of 600, 200, and 250 trajectories were calculated at 300, 1000, and 1500 K, respectively. Since the trajectories were propagated randomly in the directions of the singlet $\cdot\text{O}-\text{O}-\text{CH}_2-\text{CH}_2\cdot$ biradical IM1-s and DO, and the number of trajectories under study is fairly large, it is expected that half of the trajectories should go directly towards DO or IM1-s if barrier recrossing is unimportant. As shown in Table IV, approximately 50% of the trajectories are propagated towards both IM1-s and DO for each of the three temperatures.

A. Barrier recrossing dynamics

Non-TST barrier recrossings often occur for chemical reactions^{26,66-68} and it is of interest to determine if these dynamics are important for the trajectories initiated at TSb.

TABLE IV. Fractional yields of trajectories initiated at TSb.^a

| Temp (K) | $\cdot\text{C}_2\text{H}_4-\text{O}-\text{O}\cdot$ Pathway | Dioxetane Pathway | |
|----------|---|----------------------|-------------------------|
| | $\text{C}_2\text{H}_4 + \text{O}_2$ | Dioxetane | $2 \text{H}_2\text{CO}$ |
| 300 | 0.492(0.192) ^b | 0.505 | 0.003 |
| 1000 | 0.510(0.184) | 0.475 | 0.015 |
| 1500 | 0.448(0.184) | 0.468 | 0.084 |

^aThe trajectories were integrated for 4.5 ps. The fractions denote the final state of the trajectories.

^bThe fraction of the trajectories which form $^1\text{O}_2 + \text{C}_2\text{H}_4$ and did not form the IM1-s intermediate is given in parentheses.

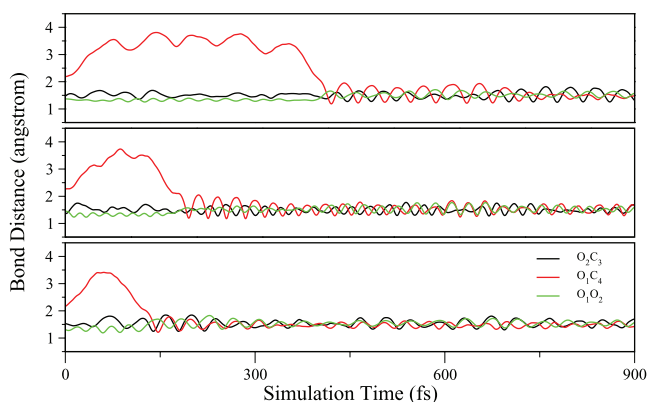


FIG. 5. Time-dependencies of the O_1-C_4 (red), O_2-C_3 (black), and O_1-O_2 (green) bond lengths for three representative trajectories initiated at TSb and which recross TSb to form dioxetane (DO) after initially moving towards the $\cdot\text{O}-\text{O}-\text{CH}_2-\text{CH}_2\cdot$ biradical intermediate (IM1-s). The trajectories in (a), (b), and (c) are for T of 300, 1000, and 1500 K, respectively.

None of the trajectories initially directed towards DO recrossed TSb, but a small number of the trajectories initially directed towards IM1-s underwent short-time barrier recrossing from IM1-s to DO; i.e. 3/298, 2/104, and 1/113 at 300, 1000, and 1500 K, respectively. Time-dependencies of the O_1-C_4 , O_2-C_3 , and O_1-O_2 bond lengths for three representative barrier recrossing trajectories are shown in Figure 5. The trajectory in (a) is initialized at 300 K and directed towards the IM1-s structure. The simulation time is 900 fs. At the beginning, the distance between the two radical terminals O_1 and C_4 increases to form IM1-s and the trajectory is trapped in the IM1-s minimum for about 300 fs; i.e., ~ 5 times the O_1-C_4 stretching vibrational period. The trajectory then crosses TSb, undergoing ring closure and forming DO within 60 fs. The formed O_1-C_4 bond is initially highly excited and energy is transferred to the O_2-C_3 bond in ~ 300 fs. The O_1-O_2 bond remains unexcited during this trajectory. Figures 5(b) and 5(c), for T of 1000 and 1500 K, respectively, show similar barrier recrossing dynamics as in (a), except the time the trajectory spends in IM1-s decreases as T is increased. For (b), as in (a), there is little excitation of the O_1-O_2 bond. For (c) this bond becomes excited as DO is formed. Overall, TS1 recrossing is unimportant for this reactive system.

B. Dynamics of trajectories moving towards IM1-s and forming $^1\text{O}_2 + \text{C}_2\text{H}_4$

As discussed above, a small fraction of the trajectories initially directed towards IM1-s recross TSb and form DO. Of interest are the dynamics of those which do not recross. All form $^1\text{O}_2 + \text{C}_2\text{H}_4$ during the 4.5 ps integration time of the trajectories, but a large fraction do not form the $\cdot\text{O}-\text{O}-\text{CH}_2-\text{CH}_2\cdot$ biradical IM1-s.

As shown in Figure 2 and Table II, for the UB3LYP/6-31G* theory used for the simulations, the energies of TSb and the $^1\text{O}_2 + \text{C}_2\text{H}_4$ products are very similar and there is a small $\sim 3 \text{ kcal/mol}$ minimum for IM1-s with respect to forming $^1\text{O}_2 + \text{C}_2\text{H}_4$. The statistical model for the reaction assumes an IM1-s intermediate is formed and then dissociates with a rate constant given by RRKM theory.³⁸ In contrast, the fraction

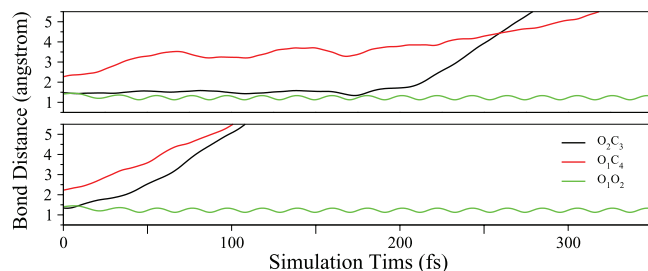


FIG. 6. Time-dependencies of the O_1-C_4 (red), O_2-C_3 (black), and O_1-O_2 (green) bond lengths for two trajectories initiated at TSb and which move directly from TSb to IM1-s: (a) a trajectory forming the $\cdot O-O-CH_2-CH_2 \cdot$ biradical intermediate IM1-s before forming $^1O_2 + C_2H_4$, $T = 1500$ K; and (b) a trajectory directly forming $^1O_2 + C_2H_4$ without first forming IM1-s, $T = 1500$ K.

of the trajectories forming $^1O_2 + C_2H_4$ without forming IM1-s is 0.39, 0.36, and 0.41 for T of 300, 1000, and 1500 K, respectively. Thus, the dynamics for forming $^1O_2 + C_2H_4$ are highly non-statistical and non-RRKM. Time-dependencies of the O_1-C_4 , O_2-C_3 , and O_1-O_2 bond lengths for trajectories forming $^1O_2 + C_2H_4$, with and without forming IM1-s, are given in Figure 6. The average lifetime of the IM1-s which are formed is 457, 214, and 164 fs for the respective temperatures of 300, 1000, and 1500 K. For comparison, the respective classical harmonic RRKM lifetimes are 200, 137, and 108 fs. The quantum harmonic RRKM lifetimes are 394, 171, and 119 fs and slightly larger. The quantum RRKM lifetimes are in better agreement with the trajectory lifetimes than are the classical RRKM lifetimes, suggesting that the short-time dynamics is vibrationally adiabatic.²⁶

The dynamics found here, that a reactive system may pass through or by a potential energy minimum without forming an intermediate, have been found in a number of other studies.⁶⁹⁻⁷² Also, the current simulation of the atomic level dynamics from TSb to $O_2 + C_2H_4$ does not allow an electronic non-adiabatic transition from the singlet to triplet PES and only $^1O_2 + C_2H_4$ is formed, with this transition allowed a fraction of the trajectories would form $^3O_2 + C_2H_4$.

C. Dynamics of dioxetane formation and dissociation: Comparison with RRKM theory

There is a significant difference between the dynamics of trajectories, initiated at TSb which initially move towards DO as compared to those which initially move towards IM1-s. All of the former form a vibrationally excited DO molecule. Plots of the O_1-C_4 , O_2-O_3 , and O_1-O_2 bond lengths versus time are shown in Figure 7 for three respective trajectories that move directly from TSb to DO; i.e., one that does not dissociate, one that dissociates at a short time, and one that dissociates at a longer time.

As shown in Table IV, the fraction of trajectories that pass the dioxetane dissociation barrier (TS1) to form two formaldehyde molecules increases from 0.33 to 8.40% as the temperature for TSb is increased from 300 to 1500 K. Similarly, the fraction of excited DO molecules which dissociate to two formaldehyde increases from 0.59 to 15.2% with this increase in temperature. These latter fractions may be inserted

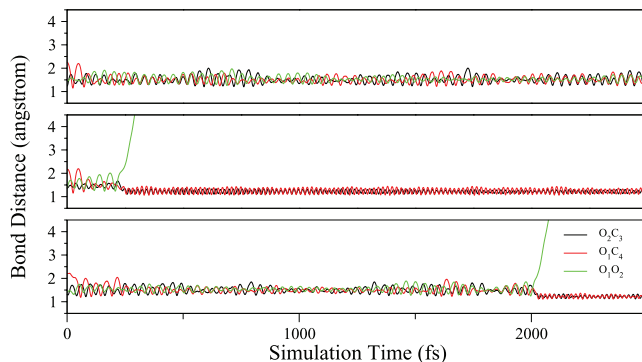


FIG. 7. Time-dependencies of the O_1-C_4 (red), O_2-C_3 (black), and O_1-O_2 (green) bond lengths for three respective trajectories initiated at TSb and which move directly to DO: (a) a trajectory that does not dissociate to two H_2CO molecules; (b) a trajectory that dissociates to two H_2CO molecules at short time; and (c) a trajectory that dissociates to two H_2CO molecules at a longer time.

into Eq. (5) to calculate the unimolecular rate constant for DO dissociation versus energy and compare with the RRKM prediction. To apply Eq. (5) to calculation the DO dissociation rate constant the time t_{DO} , for which the intramolecular vibrational dynamics of DO were followed, should be determined. This time is less than the maximum trajectory integration time t_{max} by the time Δt required by the trajectories to reach the DO potential energy minimum from TSb, where the trajectories were initiated; i.e., $t_{DO} = t_{max} - \Delta t$. As a result of the hyper-dimensional and complex phase space structure in moving from TSb to DO,⁷³⁻⁷⁵ as well as the different initial condition for each trajectory, the value of Δt is different for each trajectory. For the simulations at 300, 1000, and 1500 K, the respective ranges of Δt are 16-530, 11-318, and 12-138 fs, with average values of 44, 37, and 32 fs, respectively. Using the number of dissociations which occurred within $(t_{max} - \Delta t)$, Eq. (5), the trajectory rate constant k for dissociation of dioxetane is 1.5×10^9 , 7.0×10^9 , and $3.7 \times 10^{10} \text{ s}^{-1}$ for T of 300, 1000, and 1500 K, respectively. These values are smaller than the classical RRKM rate constant calculated from Eq. (4) by a factor of 200, 91, and 30 for T of 300, 1000, and 1500 K, respectively. Similarly, the trajectory rate constants are factors of 113, 67, and 26 times smaller than the quantum RRKM values for the respective temperatures. At short times the trajectories may retain some zero-point vibrational adiabatic properties and it is possible that a comparison with the quantum RRKM rate constants may be more appropriate.⁷⁶

The above comparisons show that the RRKM rate constants are substantially larger than those found from the trajectories. The difference with the quantum RRKM rate constants, which account for zero-point energy effects, is smaller, but the difference is still significant. The RRKM rate constants are calculated using harmonic frequencies for DO and TS1, thus, some of the difference between the trajectory and RRKM rate constants may arise from anharmonic effects.³⁸ However, a 1-2 orders of magnitude anharmonic correction to the RRKM rate constant would seem to be unusual.⁷⁷ The apparent conclusion is that RRKM theory predicts substantially more dissociation of DO than found from the trajectories.

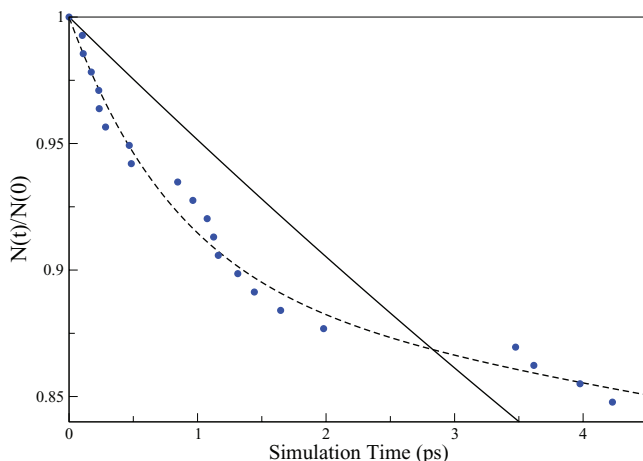


FIG. 8. Plot of $N(t)/N(0)$ versus the simulation time for the vibrational motion of dioxetane for the simulations at 1500 K. Dioxetane dissociation occurs when the trajectory reaches TS1. The solid points are the results from the simulations. The solid line is the exponential prediction of RRKM theory with the rate constant of $3.7 \times 10^{10} \text{ s}^{-1}$ determined by the number of dissociations which occurred within the integration time. The dashed line is a two exponential fit as defined by Eq. (6).

The trajectory rate constant for DO dissociation to two formaldehyde molecules will be much less than the RRKM prediction if recrossing TS1, which connects DO to the formaldehyde molecules, is important or/and if the trajectories become trapped in the phase space between TS1 and the formaldehyde products. However, neither of these dynamical possibilities occurred and instead each trajectory that passed TS1 formed the formaldehyde products without any TS1 recrossing. Thus, the non-RRKM dynamics for dioxetane dissociation apparently arises from non-statistical intramolecular vibrational dynamics within the DO phase space.

A general and important way to investigate non-RRKM dynamics for dioxetane dissociation is to study a plot of $N(t)/N(0)$ versus time.^{78–81} There are not a sufficient number of dissociating trajectories for T of 300 and 1000 K to make such a plot, but a meaningful plot can be made for the 1500 K simulation and the result is given by the solid points in Figure 8. Also included in the figure is the plot for exponential dissociation with the rate constant of $3.7 \times 10^{10} \text{ s}^{-1}$, found as described above from the total number of DO dissociations within the trajectory integration time. An important observation from Figure 8 is that $N(t)/N(0)$ is highly non-exponential and may be fit by a sum of exponentials;^{78–81} i.e.,

$$N(t)/N(0) = \sum_{i=1}^n f_i \exp(-k_i t). \quad (6)$$

The non-exponential fit given in Figure 8 is for $n = 2$, with the fitting parameters $f_1 = 0.110$ and $f_2 = 0.890$, with $k_1 = 1.17 \times 10^{12} \text{ s}^{-1}$ and $k_2 = 1.03 \times 10^{10} \text{ s}^{-1}$. The fit is not improved by using three exponentials instead of two. What is striking about the above fit is the two-orders of magnitude difference between k_1 and k_2 . The fraction of the distribution dissociating with k_1 is 0.11 and this rate constant is in overall good agreement with the respective classical and quantum RRKM values of $1.1 \times 10^{12} \text{ s}^{-1}$ and $9.5 \times 10^{11} \text{ s}^{-1}$ given in Sec. II B 2. Thus, the initial dissociation agrees with RRKM

theory. However, the bulk of the dissociation, 89%, has a rate constant two orders of magnitude smaller than the RRKM value.

Some of the non-exponential behavior of this $N(t)$ for 1500 K may arise from, the distribution of internal energy for DO which results from the distribution of energy for the trajectories initiated at TSb. However, this is not a sufficient explanation for the extensive range of rate constants in the non-exponential fits, which is much larger than the range of RRKM rate constants for the energies within the distribution. The average DO energy, as given by the discussion following Eq. (3), is a sum of the TSb ZPE, the classical potential energy release in going from TSb to DO, and the average thermal energy of TSb, $\langle E_{TSb}(T) \rangle$. The former two are fixed and their sum equals 83.8 kcal/mol. The latter arises from the Boltzmann distribution at TSb and equals 33.3 kcal/mol at 1500 K. An indication of the variation of the RRKM rate constants for the DO energy distribution at 1500 K is obtained by considering the RRKM rate constant for the 300 K simulations. Here the thermal energy of TSb is only 2.4 kcal/mol and DO is nearly monoenergetically excited. The RRKM rate constant for the average energy of this temperature is only a factor of four smaller than the RRKM rate constant for the average energy at 1500 K. In contrast the range of rate constants in the non-exponential fit to the trajectory $N(t)/N(0)$ is much larger, covering two orders of magnitude. This fit indicates that the initial DO dissociation is in approximate agreement with the RRKM prediction, but at longer times the dissociation is significantly slower than predicted by RRKM theory. Apparently there is a bottleneck⁸² for intramolecular vibrational energy redistribution⁴⁷ within DO.

D. Reaction mechanism for dioxetane dissociation

The IRC potential energy curve for dioxetane dissociation is given in Figure 3. For this model the system first reaches TS1 with an elongated O–O bond of 2.011 Å and an O–C–C–O dihedral angle of 29.5°; then passes the gauche $\cdot\text{O}-\text{CH}_2-\text{CH}_2-\text{O}\cdot$ minimum; followed by passing TS2 with a quite elongated O–O bond of 2.956 Å, a slightly elongated C–C bond of 1.596 Å, and an O–C–C–O dihedral angle of 64.7°; and then forms the two formaldehyde molecules (the geometries are those for the UB3LYP/6-31G* theory used for the simulations, see Sec. II A). For some statistical models of chemical kinetics,³⁸ an intermediate is assumed to be formed in the gauche $\cdot\text{O}-\text{CH}_2-\text{CH}_2-\text{O}\cdot$ minimum between TS1 and TS2, and then RRKM theory is used to calculate the probabilities to recross TS1 and reform DO or cross TS2 and form the formaldehyde products.

As discussed above, none of the trajectories recrossed TS1 and there was no evidence for forming an intermediate in the gauche $\cdot\text{O}-\text{CH}_2-\text{CH}_2-\text{O}\cdot$ potential energy minimum. In addition, the trajectories did not follow the IRC described above when dissociating to the two formaldehyde molecules. The ring closure reaction from TSb results in slightly stretched/excited O–O, C–O, and C–C bonds in the dioxetane molecule, with the twisting motion of the ring giving a O–C–C–O dihedral angle less than 50° before dissociation

occurs. By tracking the internal coordinates versus time for the dissociating trajectories, the C–C bond was found to cleave on average approximately only 20 fs after the O–O bond cleavage. For comparison, the vibrational periods for the O–O, C–O, and C–C stretching modes of dioxetane are ~ 25 –40 fs. For some of the trajectories there was simultaneous rupture of the O–O and C–C bonds. The O–C–C–O dihedral angle ranged from 10° to 70° , during the dissociation, although for most trajectories this angle remained between 30° and 40° . The latter values are similar to the 29.5° dihedral angle for TS1, but much smaller than the value of 64.7° for TS2, indicating the changes in this angle are not substantial in going from TS1 to TS2.

From previous work^{69–72} it is known that the reaction does not need to follow the minimum energy path given by the IRC and trajectories are not necessarily trapped in potential energy minima along this path. The dissociation of dioxetane on the singlet PES to two formaldehyde molecules occurs with these non-IRC and non-statistical dynamics.

IV. SUMMARY

The work presented here used a combination of electronic structure theory calculations and direct dynamics simulations to study the formation and decomposition of dioxetane on the ground state singlet potential energy surface. The stationary points for $^1\text{O}_2 + \text{C}_2\text{H}_4$, the singlet $\cdot\text{O}-\text{O}-\text{CH}_2-\text{CH}_2\cdot$ biradical, the transition state (TS) connecting this biradical with dioxetane, and the two transition states and gauche $\cdot\text{O}-\text{CH}_2-\text{CH}_2-\text{O}\cdot$ biradical connecting dioxetane with the formaldehyde product molecules are investigated at different levels of electronic structure theory including UB3LYP, UMP2, MRMP2, and CASSCF and a range of basis sets. The direct dynamics are performed with the UB3LYP/6-31G* method and envisage reaction of $^3\text{O}_2 + \text{C}_2\text{H}_4$ to form the triplet $\cdot\text{O}-\text{O}-\text{CH}_2-\text{CH}_2\cdot$ biradical on the ground triplet state PES. By an intersystem crossing process this biradical forms the singlet $\cdot\text{O}-\text{O}-\text{CH}_2-\text{CH}_2\cdot$ biradical on the ground state singlet PES, which can then form dioxetane by passing a TS. The direct dynamics trajectories are initiated at this TS with 300, 1000, and 1500 K Boltzmann distributions of energy and are directed towards the $\cdot\text{O}-\text{O}-\text{CH}_2-\text{CH}_2\cdot$ biradical and dioxetane. Approximately 40% of the trajectories directed towards the $\cdot\text{O}-\text{O}-\text{CH}_2-\text{CH}_2\cdot$ biradical went directly from the TS to $^1\text{O}_2 + \text{C}_2\text{H}_4$ without getting trapped and forming an intermediate in the $\cdot\text{O}-\text{O}-\text{CH}_2-\text{CH}_2\cdot$ biradical potential energy minimum, a non-statistical result. The dioxetane molecules formed dissociate to two formaldehyde molecules with a rate constant 1–2 orders of magnitude smaller than that given by RRKM theory. There is an apparent bottleneck for intramolecular vibrational energy redistribution between dioxetane's vibrational modes. The dissociation dynamics for dioxetane to the formaldehyde molecules is direct and does not involve forming a transient intermediate in the gauche $\cdot\text{O}-\text{CH}_2-\text{CH}_2-\text{O}\cdot$ biradical potential energy minimum on the IRC connecting dioxetane and the two formaldehyde molecules.

Several avenues of study could be pursued in future extensions of the work reported here. It is important to have

a deeper understanding of the nature of the intramolecular dynamics giving rise to non-statistical unimolecular decomposition for dioxetane. These dynamics are expected to be robust and unaffected by non-adiabatic transitions between the S_0 ground state studied here and the S_1 and T_1 excited states. These transitions are localized in the TS region for $\text{DO} \rightarrow 2\text{H}_2\text{CO}$ dissociation and not expected to affect the S_0 phase space structures giving rise to the non-statistical dynamics. It should be noted that molozonide has a similar near planar structure as does dioxetane and non-RRKM dynamics were also found for molozonide dissociation.⁸³ In future work there is an interest in investigating if there are relationships between the non-RRKM dynamics for dioxetane and molozonide.

The previous electronic structure calculations for the $^3\text{O}_2 + \text{C}_2\text{H}_4$ reactive system and the direct dynamics simulation reported here suggest the following mechanism for $^3\text{O}_2 + \text{C}_2\text{H}_4 \rightarrow 2\text{H}_2\text{CO}$: i.e., $^3\text{O}_2$ adds to the double bond of C_2H_4 to form the $\cdot\text{O}-\text{O}-\text{CH}_2-\text{CH}_2\cdot$ triplet biradical IM1; as a result of the high reaction barriers for IM1 on the triplet surface, it will either dissociate back to the $^3\text{O}_2 + \text{C}_2\text{H}_4$ reactants or undergo a non-adiabatic transition to form the singlet biradical IM1-s, which can either dissociate to $^1\text{O}_2 + \text{C}_2\text{H}_4$ or form DO via TSb; and DO dissociates to two formaldehyde molecules. Details of this mechanism may be studied by including in the simulations non-adiabatic transitions between S_0 and the S_1 and T_1 excited states. The rate constant for $^3\text{O}_2 + \text{C}_2\text{H}_4 \rightarrow \text{IM1-s}$ may then be determined. As discussed in Sec. II B 2, the accurate way to study the IM1-s \rightarrow DO transition in the simulations is to initiate the trajectories at the connecting transition state TSb as is done here. With electronic non-adiabatic transitions included, the branching between $^3\text{O}_2 + \text{C}_2\text{H}_4$ and $^1\text{O}_2 + \text{C}_2\text{H}_4$ may also be determined for the trajectories that move from TSb to IM1-s. In addition, it is important to consider excited electronic states, because they are intimately involved in dioxetane's decomposition.^{14–17} Both singlet and triplet state products are formed when dioxetane decomposes. Research efforts in all the above directions are planned.

ACKNOWLEDGMENTS

This material is based upon work supported by the National Science Foundation under Grant No. OISE-0730114, as part of the Partnerships in International Research and Education (PIRE) Program, and by the Robert A. Welch Foundation under Grant No. D-0005. Rui Sun is indebted to Sri-rangam V. Addepalli for his help in using the capabilities of GAMESS and parallel computing. The Hrothgar computer cluster at Texas Tech University, within the High Performance Computing Center and under the direction of Dr. Philip W. Smith, was used for the simulations reported here.

¹G. Tonachini, H. B. Schlegel, F. Bernardi, and M. A. Robb, *J. Am. Chem. Soc.* **112**, 483 (1990).

²L. B. Harding and W. A. Goddard III, *J. Am. Chem. Soc.* **102**, 439 (1980).

³A. Maranzana, G. Ghigo, and G. Tonachini, *J. Am. Chem. Soc.* **122**, 1414 (2000).

⁴C. A. Taatjes, *J. Phys. Chem. A* **110**, 4299 (2006).

- ⁵ *Combustion Chemistry*, edited by W. C. Gardiner, Jr. (Spring-Verlag, New York, 1984).
- ⁶ W. Tsang and R. F. Hampson, *J. Phys. Chem. Ref. Data* **15**, 1087 (1986).
- ⁷ W. Tsang, *J. Phys. Chem. Ref. Data* **20**, 221 (1991).
- ⁸ P. Barbe, F. Baronnet, R. Martin, and D. Perrin, *Int. J. Chem. Kinet.* **30**, 503 (1998).
- ⁹ N. D. Stothard and R. W. Walker, *J. Chem. Soc., Faraday Trans.* **87**, 241, (1991).
- ¹⁰ K. Mach, J. Novakova, V. Hanus, and Z. Dolejssek, *Collect. Czech. Chem. Commun.* **51**, 2675 (1986).
- ¹¹ T. Ingham, R. W. Walker, and R. E. Woolford, *Symp. Int. Combust. Proc.* **25**, 767 (1994).
- ¹² P. Dagaut, M. Cathonnet, and J. C. Boettner, *J. Phys. Chem.* **92**, 661 (1988).
- ¹³ A. Maranzana, G. Ghigo, G. Tonachini, and J. R. Barker, *J. Phys. Chem. A*, **112**, 3656 (2008).
- ¹⁴ C. J. Chen and J. W. Bozzelli, *J. Phys. Chem.* **104**, 9715 (2000).
- ¹⁵ H. Hua, B. Ruscic, and B. Wang, *Chem. Phys.* **311**, 335 (2005).
- ¹⁶ K. Park, A. West, E. Raheja, B. Sellner, H. Lischka, T. L. Windus, and W. L. Hase, *J. Chem. Phys.* **133**, 184306 (2010).
- ¹⁷ H. E. O'Neal and W. H. Richardson, *J. Am. Chem. Soc.* **92**, 6553 (1970).
- ¹⁸ L. B. Harding and W. A. Goddard III, *J. Am. Chem. Soc.* **99**, 4520 (1977).
- ¹⁹ W. Adam and W. J. Baader, *J. Am. Chem. Soc.* **107**, 410 (1985).
- ²⁰ N. Turro, P. Lechtken, N. E. Schore, G. Schuster, H. C. Steinmetzer, and A. Yekta, *Acc. Chem. Res.* **7**, 97 (1974).
- ²¹ W. H. Richardson and V. F. Hodge, *J. Am. Chem. Soc.* **93**, 3996 (1971).
- ²² M. Reguero, F. Bernardi, A. Bottoni, M. Olivucci, and M. A. Robb, *J. Am. Chem. Soc.* **113**, 1566 (1991).
- ²³ S. Wilsey, F. Bernardi, M. Olivucci, M. A. Robb, S. Murphy, and W. Adam, *J. Phys. Chem. A* **103**, 1699 (1999).
- ²⁴ L. De Vico, Y. Liu, J. W. Krogh, and R. Lindh, *J. Phys. Chem. A* **111**, 8013 (2007).
- ²⁵ C. Tanaka, J. Tanaka, and M. Matsumoto, *Phys. Chem. Chem. Phys.* **13**, 16005 (2011).
- ²⁶ U. Lourderaj, K. Park, and W. L. Hase, *Int. Rev. Phys. Chem.* **27**, 361 (2008).
- ²⁷ L. Sun and W. L. Hase, *Rev. Comput. Chem.* **19**, 79 (2003).
- ²⁸ A. D. Becke, *J. Chem. Phys.* **98**, 5648 (1993).
- ²⁹ P. J. Stephens, F. J. Devlin, C. F. Chabalowski, and M. J. Frisch, *J. Phys. Chem.* **98**, 11623 (1994).
- ³⁰ R. H. Hertwig and W. Koch, *Chem. Phys. Lett.* **268**, 345 (1997).
- ³¹ P. C. Hariharan and J. A. Pople, *Theoret. Chem. Acc.* **28**, 213 (1973).
- ³² M. M. Francl, W. J. Pietro, W. J. Hehre, J. S. Binkley, M. S. Gordon, D. J. DeFrees, and J. A. Pople, *J. Chem. Phys.* **77**, 3654 (1982).
- ³³ B. O. Roos, *Adv. Chem. Phys.* **69**, 399 (1987).
- ³⁴ M. W. Schmidt and M. S. Gordon, *Annu. Rev. Phys. Chem.* **48**, 233 (1998).
- ³⁵ K. Hirao, *Chem. Phys. Lett.* **190**, 374 (1992).
- ³⁶ H. Nakano, *J. Chem. Phys.* **99**, 7983 (1993).
- ³⁷ T. H. Dunning, Jr., *J. Chem. Phys.* **90**, 1007 (1989).
- ³⁸ T. Baer and W. L. Hase, *Unimolecular Reaction Dynamics. Theory and Experiments* (Oxford University Press, New York, 1996).
- ³⁹ C. M. Aikens, S. P. Webb, R. L. Bell, G. D. Fletcher, M. W. Schmidt, and M. S. Gordon, *Theoret. Chem. Acc.* **110**, 233 (2003).
- ⁴⁰ R. Ditchfield, W. J. Hehre, and J. A. Pople, *J. Chem. Phys.* **54**, 724 (1971).
- ⁴¹ W. J. Hehre, R. Ditchfield, and J. A. Pople, *J. Chem. Phys.* **56**, 2257 (1972).
- ⁴² R. Krishnan, J. S. Binkley, R. Seeger, and J. A. Pople, *J. Chem. Phys.* **72**, 650 (1980).
- ⁴³ K. Fukui, *J. Phys. Chem.* **74**, 4161 (1970).
- ⁴⁴ D. L. Bunker, *J. Chem. Phys.* **37**, 393 (1962).
- ⁴⁵ N. C. Blais and D. L. Bunker, *J. Chem. Phys.* **37**, 2713 (1962).
- ⁴⁶ L. Yang, R. Sun, and W. L. Hase, *J. Chem. Theory Comput.* **7**, 3478 (2011).
- ⁴⁷ W. L. Hase, *J. Phys. Chem.* **90**, 365 (1986).
- ⁴⁸ S. K. Gray, D. W. Noid, and B. G. Sumpter, *J. Chem. Phys.* **101**, 4062 (1994).
- ⁴⁹ T. Schlick, *Molecular Modeling and Simulation* (Springer, New York, 2000).
- ⁵⁰ Ch. Schlier and A. Seiter, *J. Phys. Chem. A* **102**, 9399 (1998).
- ⁵¹ A. Szalbo and N. S. Ostlund, *Modern Quantum Chemistry, Introduction to Advanced Electronic Structure Theory* (Dover, New York, 1996).
- ⁵² W. L. Hase, R. J. Duchovic, X. Hu, A. Komornicki, K. F. Lim, D. H. Lu, G. H. Peslherbe, S. R. Swamy, S. R. Vande Linde, A. Varandas, *et al.*, *QCPE Bull.* **16**, 671 (1996).
- ⁵³ X. Hu, W. L. Hase, and T. Pirraglia, *J. Comput. Chem.* **12**, 1014 (1991).
- ⁵⁴ M. Valiev, E. J. Bylaska, N. Govind, K. Kowalski, T. P. Straatsma, H. J. J. van Dam, D. Wang, J. Nieplocha, E. Apra, T. L. Windus, and W. A. de Jong, *Comput. Phys. Commun.* **181**, 1477 (2010).
- ⁵⁵ M. W. Schmidt, K. K. Baldrige, J. A. Boatz, S. T. Elbert, M. S. Gordon, J. H. Jensen, S. Koseki, N. Matsunaga, K. A. Nguyen, S. Su, T. L. Windus, M. Dupuis, and J. A. Montgomery, *J. Comput. Chem.* **14**, 1341 (1993).
- ⁵⁶ S. Hammes-Schiffer and J. C. Tully, *J. Chem. Phys.* **103**, 8528 (1995).
- ⁵⁷ Y. Zhao, G. Mil'nikov, and H. Nakamura, *J. Chem. Phys.* **121**, 8854 (2004).
- ⁵⁸ J. I. Steinfeld, J. S. Francisco, and W. L. Hase, *Chemical Kinetics and Dynamics*, 2nd ed. (Prentice Hall, Upper Saddle River, NJ, 1999), p. 316.
- ⁵⁹ L. Sun, K. Park, K. Song, D. W. Setser, and W. L. Hase, *J. Chem. Phys.* **124**, 64313 (2006).
- ⁶⁰ D. L. Bunker and E. A. Goring-Simpson, *Faraday Discuss. Chem. Soc.* **55**, 93 (1973).
- ⁶¹ G. H. Peslherbe, H. Wang, and W. L. Hase, *Adv. Chem. Phys.* **105**, 171 (1999).
- ⁶² L. Zhu and W. L. Hase, *Chem. Phys. Lett.* **175**, 117 (1990).
- ⁶³ L. Zhu, W. Chen, W. L. Hase, and E. W. Kaiser, *J. Phys. Chem.* **97**, 311 (1993).
- ⁶⁴ L. Zhu and W. L. Hase, *QCPE Bull.* **14**, 644 (1994).
- ⁶⁵ W. L. Hase and D. G. Buckowski, *J. Comput. Chem.* **3**, 335 (1982).
- ⁶⁶ Y. J. Cho, S. R. Vande Linde, L. Zhu, and W. L. Hase, *J. Chem. Phys.* **96**, 8275 (1992).
- ⁶⁷ H. Wang, G. H. Peslherbe, and W. L. Hase, *J. Am. Chem. Soc.* **116**, 9644 (1994).
- ⁶⁸ L. Sun, W. L. Hase, and K. Song, *J. Am. Chem. Soc.* **123**, 5753 (2001).
- ⁶⁹ S. R. Vande Linde and W. L. Hase, *J. Am. Chem. Soc.* **111**, 2349 (1989).
- ⁷⁰ C. Doubleday, Jr., K. Bolton, and W. L. Hase, *J. Phys. Chem. A* **102**, 3648 (1998).
- ⁷¹ L. Sun, K. Song, and W. L. Hase, *Science* **296**, 875 (2002).
- ⁷² J. G. López, G. Vayner, U. Lourderaj, S. V. Addepalli, S. Kato, W. A. de Jong, T. L. Windus, and W. L. Hase, *J. Am. Chem. Soc.* **129**, 9976 (2007).
- ⁷³ A. J. Lichtenberg and M. A. Lieberman, *Regular and Stochastic Motion* (Springer, New York, 1983).
- ⁷⁴ P. Pechukas, *Ann. Rev. Phys. Chem.* **32**, 159 (1981).
- ⁷⁵ M. J. Davis, *J. Chem. Phys.* **83**, 1016 (1985).
- ⁷⁶ S. Y. Grebenshchikov, R. Schinke, and W. L. Hase, *Comprehensive Chemical Kinetics, Unimolecular Kinetics Part 1. The Reaction Step*, edited by N. J. B. Green (Elsevier Science, Amsterdam, 2003), Vol. 39, pp. 105–242.
- ⁷⁷ K. Song and W. L. Hase, *J. Chem. Phys.* **110**, 6198 (1999).
- ⁷⁸ W. L. Hase, R. J. Duchovic, K. N. Swamy, and R. J. Wolf, *J. Chem. Phys.* **80**, 714 (1984).
- ⁷⁹ R. A. Marcus, W. L. Hase, and K. N. Swamy, *J. Phys. Chem.* **88**, 6717 (1984).
- ⁸⁰ S. R. Vande Linde and W. L. Hase, *J. Chem. Phys.* **93**, 7962 (1990).
- ⁸¹ G. H. Peslherbe, H. Wang, and W. L. Hase, *J. Chem. Phys.* **102**, 5626 (1995).
- ⁸² D. L. Bunker and W. L. Hase, *J. Chem. Phys.* **59**, 4621 (1973).
- ⁸³ G. Vayner, S. V. Addepalli, K. Song, and W. L. Hase, *J. Chem. Phys.* **125**, 014317 (2006).